

NOVEL GRADIENT-ENHANCED MULTI-FIDELITY SURROGATE MODEL ASSISTED ROBUST MULTIDISCIPLINARY DESIGN OPTIMIZATION OF TAILLESS FLYING WING

Zhao Huan, Wang She-kun, Gong Zhi-yuan, Gan Ke-yao,

School of Aeronautics, Northwestern Polytechnical University, Xi'an Shaanxi, 710072, P. R. China

Abstract

The tailless flying wing is one of the best configurations combining the high aerodynamic and stealth characteristics, but the lack of longitudinal control poses a significant challenge to aerodynamic shape optimization (ASO) of such configuration. Currently, the adjoint-based optimization method cannot meet the needs of multi-objective global optimization for aerodynamic/stealth/control multidisciplinary design, while the surrogate-based global optimization method faces these problems such as increased computational cost and poor generalization ability. In order to tackle this thorny problem, this paper establishes an efficient global aerodynamic/stealth multidisciplinary robust design optimization method based on the proposed gradientenhanced multi-fidelity polynomial chaos-Kriging (GEMF-PCK) surrogate model. The GEMF-PCK model utilizes the inexpensive gradient information, such as an adjoint method, as an auxiliary to enhance the adaptive multi-level multi-fidelity surrogate modelling. The partial least squares method is used to reduce the number of hyperparameters with the number of independent variables. This GEMF-PCK model was validated to be capable of improving modeling efficiency and global generalization for aerodynamic problems with highdimensional independent variables. An adaptive multi-fidelity sequential sampling technique based on leaveone-out cross validation- Voronoi maximin scaled distance (LOOCV-Voronoi-MSD) and an efficient singlecycle robust design optimization method based on the GEMF-PCK model are developed, which further improves the efficiency of multi-objective robust design optimization of the tailless flying wing. To examine the overall performance of the developed method, we apply it to the aerodynamic/stealth multidisciplinary design of the tailless flying wing. The results show that the developed aerodynamic/stealth multi-objective robust design optimization method significantly improves the optimization efficiency, meeting the needs of efficient aerodynamic/stealth design for the future tailless flying wing. The optimized new shape reduces the average drag by more than 20 counts over a wide Mach number range compared to the initial layout, increases the Mach number of drag divergence by 0.03, and significantly improves the robustness of drag coefficient. The longitudinal moment coefficient of the whole aircraft reaches self-leveling, and the reliability is also significantly higher. At the same time, stealth analysis shows that compared to the initial layout, the optimized layout reduces the average radar cross section (RCS) by more than 90% in the L, S, C, X bands, and reduces the forward RCS by more than one order of magnitude, resulting in comprehensive improvement in stealth characteristics, which can meet the needs of future high-stealthy flying wing layout aircraft for all-directional and all-frequency stealthy use.

Keywords: gradient-enhanced multi-level multi-fidelity polynomial chaos-Kriging (GEMLMF-PCK), flying wing, robust aerodynamic/stealth design optimization, multi-fidelity sequential sampling, multi-fidelity surrogate model.

1. Introduction

With the continuously increasing requirements for performance and fidelity for aerodynamic shape optimization (ASO), higher-fidelity CFD numerical simulations are expected to be applied in ASO. This leads to a sharp increase in computational costs for CFD analysis of the same number of samples, and therefore there is an urgent demand to develop more efficient surrogate optimization methods [1-4]. One of the most popular methods for this is to use a multi-fidelity surrogate model instead of the original single-fidelity surrogate model to reduce the number of high-fidelity samples used in the surrogate modelling and optimization process. The multi-fidelity surrogate model captures the trend of the physical model by building a low-fidelity (LF) model using a large number of inexpensive low-fidelity samples, and corrects the LF model using a small number of high-fidelity (HF) samples, which significantly reduces the computational cost required to construct a HF surrogate model and improving the efficiency of surrogate modeling and surrogate-based optimization (SBO)[5-7]. However, the insufficient generalization ability of multi-fidelity surrogate models also seriously affects the performance of SBO algorithms[8, 9]. In order to improve the performance of multi-fidelity surrogate-based optimization algorithms, one of the potential solutions to this problem is to improve the generalization ability of multi-fidelity surrogate models. As proved, currently popular multi-fidelity surrogate models, such as co Kriging^[10] and multi-fidelity polynomial chaos expansion (MF-PCE)[11], exhibit significant differences in performance across different problems^[6, 12]. What's worse, if used improperly, their performance of modeling and optimization may be poor. Based on this reason, an adaptive multi-fidelity polynomial chaos-Kriging (AMF-PCK) surrogate model was proposed previously to solve this problem of poor generalization ability for multi-fidelity surrogate models^[13-15]. Further, the AMF-PCK surrogate model has been validated by using complex numerical functions and aerodynamic data modeling problems, demonstrating that the AMF-PCK model have stronger generalization ability and higher modeling efficiency for high nonlinear/high-order responses than the popular universal Kriging, MF-PCE and Co-Kriging models[13-

However, with the increasing requirements for the performance and fidelity of aerodynamic shape global optimization, which requires the use of high-fidelity CFD numerical simulations and hundreds of independent design variables (DVs) to describe the aerodynamic shape, which leads to a higher computational cost, a longer design cycle, and a severer challenge of the curse of dimensionality for SBO methods^[14, 16-21]. What's worse, the curse of dimensionality also continues to be an obstacle for the further development of multi-fidelity surrogate models. For an example, high-dimensional DVs will cause a sharp increase of the correlation matrix size of the classical Co-kriging model, so that the hyperparameter optimization process is longer and the convergence deteriorates in the modelling process. For another example, the number of candidate polynomial terms in MF-PCE models increases with the increasing polynomial order and the number of DVs, which leads to a longer training time, making it difficult to efficiently establish multi-fidelity surrogate models involving highdimensional DVs [11]. Aiming at alleviating the curse of dimensionality, one of the most potential solutions is to embed gradient information into the multi-fidelity surrogate model. This article first introduces the modelling process of the gradient-enhanced multi-fidelity polynomial chaos-Kriging surrogate (GEMF-PCK) model. Such method adaptively selects the optimal polynomial basis function, their gradient information as well as constructs the optimal multi-fidelity surrogate model by combining the global approximation characteristics of PCE and the local interpolation characteristics of Kriging. As a result, the global modeling efficiency and generalization ability of the GEMF-PCK surrogate model for high-dimensional DVs will be significantly improved with the cheap gradient information being utilized, especially in terms of the approximation accuracy for complex responses such as high-order/high-nonlinear problems, greatly expanding the application scope and adaptability of multi-fidelity surrogate models. To test the performance of the new method, this paper applies it to the robust aerodynamic/stealth design of tailless flying wing shape. Results demonstrate that the GEMF-PCK assisted robust aerodynamic/stealth design method significantly improves the optimization efficiency as well as effectively balancing the performance and robustness of the aerodynamic and stealth characteristics, meeting the needs of efficient aerodynamic/stealth design for the future tailless flying wing. This method lays the foundation for the future development of robust multi-disciplinary design optimization of aircrafts for high-dimensional DVs as well as also provides new ideas for solving the problem of the poor adaptability of current multi-fidelity surrogate optimization algorithms.

2. Gradient-enhanced multi-fidelity polynomial chaos-Kriging surrogate model

The gradient-enhanced multi-fidelity polynomial chaos-Kriging (GEMF-PCK) surrogate model is derived from the previously proposed adaptive multi-fidelity polynomial chaos-Kriging (AMF-PCK) model^[13] by incorporating the gradient information. The GEMF-PCK model will provide better generation ability for a function with high-dimensional inputs.

2.1 Gradient-enhanced polynomial chaos-Kriging model for low-fidelity approximation

For a polynomial chaos-Kriging surrogate model, the low-fidelity response $y_l(\mathbf{X})$ at a given point \mathbf{X} can be considered as a realization of Gaussian process namely

$$y_l(\mathbf{X}) = \sum_{i=1}^{M} \beta_{r_i} \psi_{r_i}(\mathbf{X}) + z_l(\mathbf{X}),$$
(1)

where the sparse PC bases $\{\psi_{r_i}(\mathbf{X})\}_{i=1}^M$ $(M \leq \min{(M_p, N_l)})$ are first selected by the LAR algorithm and then used as the trend functions. Here M denotes the number of selected polynomial bases and the coefficient vector $\mathbf{\beta}_r = (\beta_{r_1}, \beta_{r_2}, \cdots, \beta_{r_M})^\mathrm{T}$. To build a gradient-enhanced polynomial chaos-Kriging (GEPCK) surrogate model, a training sample is generated, denoted as $\mathbf{S}_l = \{\mathbf{X}^{(1)}, \mathbf{X}^{(2)}, \cdots, \mathbf{X}^{(N_l)}\}$. Their responses and gradient information are calculated by the LF model, defined in

$$\dot{\mathbf{Y}}_{l} = \left(y_{l}(\mathbf{X}^{(1)}), y_{l}(\mathbf{X}^{(2)}), \dots, y_{l}(\mathbf{X}^{(N_{l})}), \frac{\partial y_{l}(\mathbf{X}^{(1)}))}{\partial x_{1}}, \dots, \frac{\partial y_{l}(\mathbf{X}^{(1)}))}{\partial x_{n}}, \dots, \frac{\partial y_{l}(\mathbf{X}^{(N_{l})}))}{\partial x_{1}}, \dots, \frac{\partial y_{l}(\mathbf{X}^{(N_{l})}))}{\partial x_{n}}\right)^{\mathrm{T}} (2)$$

With a size of $N_l(n+1) \times 1$, Here, N_l and n represent the LF training sample size and dimension, respectively. By incorporating the gradient information, the augmented correlation matrix $\dot{\mathbf{R}}_l$ reads as

$$\dot{\mathbf{R}}_{l} = \begin{bmatrix} R_{l}(\mathbf{X}^{(1)}, \mathbf{X}^{(1)}) & \cdots & R_{l}(\mathbf{X}^{(1)}, \mathbf{X}^{(N_{l})}) & \frac{\partial R_{l}(\mathbf{X}^{(1)}, \mathbf{X}^{(1)})}{\partial x_{1}} & \cdots & \frac{\partial R_{l}(\mathbf{X}^{(1)}, \mathbf{X}^{(1)})}{\partial x_{n}} & \cdots & \frac{\partial R_{l}(\mathbf{X}^{(N_{l})}, \mathbf{X}^{(N_{l})})}{\partial x_{n}} \\ \vdots & \ddots & \vdots & \ddots & \vdots & \ddots & \vdots \\ R_{l}(\mathbf{X}^{(N_{l})}, \mathbf{X}^{(1)}) & \cdots & R_{l}(\mathbf{X}^{(N_{l})}, \mathbf{X}^{(N_{l})}) & \frac{\partial R_{l}(\mathbf{X}^{(N_{l})}, \mathbf{X}^{(1)})}{\partial x_{1}} & \cdots & \frac{\partial R_{l}(\mathbf{X}^{(N_{l})}, \mathbf{X}^{(1)})}{\partial x_{n}} & \cdots & \frac{\partial R_{l}(\mathbf{X}^{(N_{l})}, \mathbf{X}^{(N_{l})})}{\partial x_{n}} \\ \vdots & \ddots & \vdots & \ddots & \vdots & \ddots & \vdots \\ \frac{\partial R_{l}(\mathbf{X}^{(1)}, \mathbf{X}^{(1)})}{\partial x_{n}} & \cdots & \frac{\partial R_{l}(\mathbf{X}^{(1)}, \mathbf{X}^{(N_{l})})}{\partial x_{n}} & \frac{\partial R_{l}(\mathbf{X}^{(1)}, \mathbf{X}^{(1)})}{\partial x_{n}} & \frac{\partial R_{l}(\mathbf{X}^{(1)}, \mathbf{X}^{(1)})}{\partial x_{n}} & \cdots & \frac{\partial R_{l}(\mathbf{X}^{(N_{l})}, \mathbf{X}^{(N_{l})})}{\partial x_{n}} \\ \vdots & \ddots & \vdots & \ddots & \vdots & \ddots & \vdots \\ \frac{\partial R_{l}(\mathbf{X}^{(N_{l})}, \mathbf{X}^{(1)})}{\partial x_{n}} & \cdots & \frac{\partial R_{l}(\mathbf{X}^{(N_{l})}, \mathbf{X}^{(N_{l})})}{\partial x_{n}} & \frac{\partial R_{l}(\mathbf{X}^{(1)}, \mathbf{X}^{(1)})}{\partial x_{n}\partial x_{1}} & \cdots & \frac{\partial R_{l}(\mathbf{X}^{(N_{l})}, \mathbf{X}^{(N_{l})})}{\partial x_{n}\partial x_{n}} \\ \vdots & \vdots & \vdots & \ddots & \vdots & \ddots & \vdots \\ \frac{\partial R_{l}(\mathbf{X}^{(N_{l})}, \mathbf{X}^{(1)})}{\partial x_{n}} & \cdots & \frac{\partial R_{l}(\mathbf{X}^{(N_{l})}, \mathbf{X}^{(N_{l})})}{\partial x_{n}\partial x_{1}} & \cdots & \frac{\partial R_{l}(\mathbf{X}^{(N_{l})}, \mathbf{X}^{(N_{l})})}{\partial x_{n}\partial x_{n}} \\ \frac{\partial R_{l}(\mathbf{X}^{(N_{l})}, \mathbf{X}^{(N_{l})})}{\partial x_{n}\partial x_{n}} & \cdots & \frac{\partial R_{l}(\mathbf{X}^{(N_{l})}, \mathbf{X}^{(N_{l})})}{\partial x_{n}\partial x_{1}} & \cdots & \frac{\partial R_{l}(\mathbf{X}^{(N_{l})}, \mathbf{X}^{(N_{l})})}{\partial x_{n}\partial x_{n}} \\ \frac{\partial R_{l}(\mathbf{X}^{(N_{l})}, \mathbf{X}^{(N_{l})})}{\partial x_{n}\partial x_{1}} & \cdots & \frac{\partial R_{l}(\mathbf{X}^{(N_{l})}, \mathbf{X}^{(N_{l})})}{\partial x_{n}\partial x_{1}} & \cdots & \frac{\partial R_{l}(\mathbf{X}^{(N_{l})}, \mathbf{X}^{(N_{l})})}{\partial x_{n}\partial x_{n}} \\ \frac{\partial R_{l}(\mathbf{X}^{(N_{l})}, \mathbf{X}^{(N_{l})})}{\partial x_{n}\partial x_{1}} & \cdots & \frac{\partial R_{l}(\mathbf{X}^{(N_{l})}, \mathbf{X}^{(N_{l})})}{\partial x_{n}\partial x_{1}} & \cdots & \frac{\partial R_{l}(\mathbf{X}^{(N_{l})}, \mathbf{X}^{(N_{l})})}{\partial x_{n}\partial x_{n}} \\ \frac{\partial R_{l}(\mathbf{X}^{(N_{l})}, \mathbf{X}^{(N_{l})})}{\partial x_{n}\partial x_{1}} & \cdots & \frac{\partial R_{l}(\mathbf{X}^{(N_{l})}, \mathbf{X}^{(N_{l})})}{\partial x_{n}\partial x_{1}} & \cdots & \frac{\partial R_{l}(\mathbf{X}^{(N_{l})}, \mathbf{X}^{(N_{l})})}{\partial x_{n}\partial x_{n}} \\ \frac{\partial R_{l}(\mathbf{X}^{(N_{l})}, \mathbf{$$

By utilizing the selected polynomial set as the trend functions, the universal Kriging regression is performed, which includes the calibration of hyper-parameters $\{ {m \theta}_l, q_l \}$ by maximum likelihood estimation (MLE) [22] (or LOOCV [23]) and PCK fitting with calibrated parameters $\{ {m \theta}_l, q_l, \sigma_{z_l}^2, \dot{{\bf \beta}}_r \}$ is performed. The optimal hyper-parameters are estimated by minimizing the condensed likelihood expression

$$\left\{\mathbf{\theta}_{l}, q_{l}\right\}_{ML} = \underset{\mathbf{\theta}_{l}, q_{l}}{\operatorname{arg min}} \left(\sigma_{z_{l}}^{2} \left|\dot{\mathbf{R}}_{l}\right|^{1/N_{l}}\right), \ \theta_{l_{i}} > 0, q_{l} > 0,$$

$$(4)$$

where $\dot{\mathbf{R}}_l$ is a augmented correlation matrix defined in Eq. (3). The process variance $\sigma_{z_l}^2$ is estimated by $\sigma_{z_l}^2 = (\dot{\mathbf{Y}}_l - \dot{\mathbf{\Psi}}_r \dot{\mathbf{\beta}}_r)^{\mathrm{T}} \mathbf{R}_l^{-1} (\dot{\mathbf{Y}}_l - \dot{\mathbf{\Psi}}_r \dot{\mathbf{\beta}}_r)/N_l$, where the measure matrices $\dot{\mathbf{\Psi}}_r \in \mathbb{R}^{N_l(n+1)\times M(n+1)}$ are defined as

$$\dot{\boldsymbol{\Psi}}_{r}(\mathbf{X}) = \begin{bmatrix} \boldsymbol{\psi}_{r}(\mathbf{X}^{(1)}) & \frac{\partial \boldsymbol{\psi}_{r}(\mathbf{X}^{(1)})}{\partial x_{1}} & \cdots & \frac{\partial \boldsymbol{\psi}_{r}(\mathbf{X}^{(1)})}{\partial x_{n}} \\ \boldsymbol{\psi}_{r}(\mathbf{X}^{(2)}) & \frac{\partial \boldsymbol{\psi}_{r}(\mathbf{X}^{(2)})}{\partial x_{1}} & \cdots & \frac{\partial \boldsymbol{\psi}_{r}(\mathbf{X}^{(2)})}{\partial x_{n}} \\ \vdots & \vdots & \ddots & \vdots \\ \boldsymbol{\psi}_{r}(\mathbf{X}^{(N_{l})}) & \frac{\partial \boldsymbol{\psi}_{r}(\mathbf{X}^{(N_{l})})}{\partial x_{1}} & \cdots & \frac{\partial \boldsymbol{\psi}_{r}(\mathbf{X}^{(N_{l})})}{\partial x_{n}} \end{bmatrix} \in \mathbb{R}^{N_{l}(n+1) \times M(n+1)}, \tag{5}$$

$$\boldsymbol{\psi}_{r}(\mathbf{X}) = \begin{bmatrix} \boldsymbol{\psi}_{r_{1}}(\mathbf{X}) & \boldsymbol{\psi}_{r_{2}}(\mathbf{X}) & \cdots & \boldsymbol{\psi}_{r_{M}}(\mathbf{X}) \end{bmatrix}$$

and $\psi_r(\mathbf{X})$ are computed by substituting the low-fidelity samples sites \mathbf{S}_l into the selected polynomial basis set $\{\psi_{r_l}(\mathbf{X})\}_{l=1}^M$. With hyper-parameters $\{\mathbf{\theta}_l,q_l\}$ determined, the coefficient vector $\dot{\mathbf{\beta}}_r$ is calculated by the generalized least squares (GLSE), namely $\dot{\mathbf{\beta}}_r = (\dot{\mathbf{\Psi}}_r^T \dot{\mathbf{R}}_l^{-1} \dot{\mathbf{\Psi}}_r)^{-1} \dot{\mathbf{\Psi}}_r^T \dot{\mathbf{R}}_l^{-1} \dot{\mathbf{Y}}_l = [\beta_{r_1},\cdots,\beta_{r_M},\beta_{r_{1,1}},\cdots,\beta_{r_{M,n}}]$. Then, according to the universal Kriging fitting process [24], the PCK predictor corresponding to the LF function at any untried point \mathbf{X} is obtained by

$$\hat{y}_{l}(\mathbf{X}) = \sum_{i=1}^{M} \beta_{r_{i}} \psi_{r_{i}}(\mathbf{X}) + \sum_{j=1}^{n} \sum_{i=1}^{M} \beta_{r_{i,j}} \frac{\partial \psi_{r_{i}}(\mathbf{X})}{\partial x_{i}} + \dot{\mathbf{r}}_{l}^{\mathrm{T}} \dot{\mathbf{R}}_{l}^{-1} (\dot{\mathbf{Y}}_{l} - \dot{\mathbf{\Psi}}_{r} \boldsymbol{\beta}_{r}), \tag{6}$$

wherein, the augmented correlation vector $\dot{\mathbf{r}}_l \in \mathbb{R}^{N_l \times (1+n)}$ represents the correlation between the untried point and the observed sample sites \mathbf{S}_l , namely

$$\dot{\mathbf{r}}_{l}(\mathbf{X}) = \left\{ \mathbf{r}_{l}(\mathbf{X}) \quad \frac{\partial \mathbf{r}_{l}(\mathbf{X})}{\partial x_{1}} \quad \cdots \quad \frac{\partial \mathbf{r}_{l}(\mathbf{X})}{\partial x_{n}} \right\}^{\mathrm{T}}$$

$$\mathbf{r}_{l}(\mathbf{X}) = \left[R(\mathbf{X}^{(1)}, \mathbf{X}), R(\mathbf{X}^{(2)}, \mathbf{X}), \cdots, R(\mathbf{X}^{(N_{l})}, \mathbf{X}) \right]^{\mathrm{T}}$$
(7)

2.2 GEMF-PCK with gradient information

In this work, the GEMF-PCK metamodel for approximating HF function $y_h(\mathbf{X})$ is built by using a combined correction form for the low-fidelity (LF) PCK model and incorporating gradient information, as given by

$$y_h(\mathbf{X}) = \alpha_0 \hat{y}_l(\mathbf{X}) + \underbrace{y_c(\mathbf{X}) + z_h(\mathbf{X})}_{C(\mathbf{X})},$$
(8)

where α_0 is the multiplicative correction factor to indicate the correlation between low-and high-fidelity models and avoid the bumpy issue ^[25]. The symbol $\hat{y}_l(\mathbf{X})$ represents the low-fidelity polynomial chaos-Kriging predictor. $C(\mathbf{X})$ is the additive correction term, which uses an adaptive correction polynomial expansion- Gaussian process to accurately approximate the complex difference between scaling low-fidelity model $(\alpha_0 \hat{y}_l(\mathbf{X}))$ and high-fidelity model $(y_h(\mathbf{X}))$.

In this work, we first obtain sparse PC representations with the least angle regression (LAR) algorithm using LF computations, with a limited number of significant coefficients available in the

GE-MFSM ASSISTED RMDO OF TAILLESS FLYING WING

expansion that may correspond to the low- or high-order basis. We assume that the relative importance of PC terms and the relative strengths of corresponding polynomial coefficients are provided by the first LAR-PCK metamodeling using LF computations. Then a subset of the coefficients of these significant PC terms is corrected using the high-fidelity data to improve the approximation accuracy. Further, the correction expansion $y_c(\mathbf{X})$ from the sparse PCE with gradient information is expressed by

$$y_c(\mathbf{X}) = \sum_{c_i \in A_c} \alpha_{c_i} \psi_{c_i}(\mathbf{X}) + \sum_{c_i \in A_c} \sum_{j=1}^n \alpha_{c_{i,j}} \frac{\partial \psi_{c_i}(\mathbf{X})}{\partial x_j}, \tag{9}$$

where A_c and $\alpha_{c,>}$ are the index set of the correction polynomial expansion and the corresponding polynomial coefficients, respectively. The polynomial term in the correction expansion has to be a subset of the LF expansion. The cardinality of A_c should be smaller than the cardinality of the set A, where $A = \{r_1, r_2, \cdots, r_M\}$ is the index set of selected PC terms in $\hat{y}_l(\mathbf{X})$, namely $A_c \subseteq A$. Substitute Eq. (9) into Eq. (8), we can get the general expression of the GEMF-PCK metamodel namely

$$y_{h}(\mathbf{X}) = \alpha_{0} \underbrace{\left(\sum_{i=1}^{M} \beta_{r_{i}} \psi_{r_{i}}(\mathbf{X}) + \sum_{j=1}^{n} \sum_{i=1}^{M} \beta_{r_{i,j}} \frac{\partial \psi_{r_{i}}(\mathbf{X})}{\partial x_{j}} + \dot{\mathbf{r}}_{l}^{\mathrm{T}} \dot{\mathbf{R}}_{l}^{-1} (\dot{\mathbf{Y}}_{l} - \dot{\boldsymbol{\Psi}}_{r} \boldsymbol{\beta}_{r}) \right)}_{\hat{y}_{l}(\mathbf{X})} + \underbrace{\left(\sum_{c_{i} \in A_{c}} \alpha_{c_{i}} \psi_{c_{i}}(\mathbf{X}) + \sum_{c_{i} \in A_{c}} \sum_{j=1}^{n} \alpha_{c_{i,j}} \frac{\partial \psi_{c_{i}}(\mathbf{X})}{\partial x_{j}} + z_{h}(\mathbf{X}) \right)}_{\hat{y}_{l}(\mathbf{X})}, (10)$$

where the multiplicative correction factor α_0 and the correction expansion coefficients α_{c_i} should be explicitly tuned to make them well-suited for design and analysis of computer experiments (the procedure is detailed in Section 2.3).

2.3 Fitting of gradient enhanced multi-fidelity polynomial chaos-Kriging

The GEMF-PCK model is built by the assumption of minimizing the mean-squared error (MSE) and unbiased estimation, as is similar with the universal Kriging modeling. It is assumed that the HF function value at given point \mathbf{X} can be approximated by a linear combination of the observed HF data \mathbf{Y}_h , namely

$$\hat{\mathbf{y}}_h(\mathbf{X}) = \mathbf{w}^{\mathrm{T}} \dot{\mathbf{Y}}_h,\tag{11}$$

where $\mathbf{w}=(w_1,w_2,\cdots,w_{N_h})^{\mathrm{T}}$ is the coefficients vector, The HF observed data with gradient information reads as $\mathbf{Y}_h=(y_h(\mathbf{X}^{(1)}),y_h(\mathbf{X}^{(2)}),\cdots,y_h(\mathbf{X}^{(N_h)}),\cdots,\frac{\partial y_h(\mathbf{X}^{(1)})}{\partial x_1},\cdots,\frac{\partial y_h(\mathbf{X}^{(1)})}{\partial x_n},\cdots,\frac{\partial y_h(\mathbf{X}^{(N_h)})}{\partial x_1},\cdots,\frac{\partial y_$

$$\hat{\mathbf{y}}_h(\mathbf{X}) - \mathbf{y}_h(\mathbf{X}) = \mathbf{w}^{\mathrm{T}} \mathbf{Y}_h - (\alpha_0 \hat{\mathbf{y}}_l(\mathbf{X}) + \mathbf{y}_c(\mathbf{X}) + \mathbf{z}_h(\mathbf{X})). \tag{12}$$

where $\hat{y}_l(\mathbf{X})$ is firstly fitted, and $y_c(\mathbf{X})$ is determined as presented in Section 1.1. The GEMF-PCK metamodel is desired to meet the following formulation:

$$Min\left(E\left(\left(\hat{y}_h(\mathbf{X}) - y_h(\mathbf{X})\right)^2\right)\right),\tag{13}$$

subjected to the constraint of unbiased estimation:

$$E(\hat{y}_h(\mathbf{X}) - y_h(\mathbf{X})) = 0. \tag{14}$$

The constrained minimization problem, namely empirical best linear unbiased predictor (BLUP), can be solved by the Lagrange multiplier approach [26] to obtain the vector of weight coefficients $\mathbf{w} =$

 $(w_1, w_2, \dots, w_{N_h})^T$, as expressed in the matrix form:

$$\begin{bmatrix} \mathbf{R}_h & \mathbf{F} \\ \mathbf{F}^T & \mathbf{0} \end{bmatrix} \begin{bmatrix} \mathbf{w} \\ \tilde{\lambda} \end{bmatrix} = \begin{bmatrix} \mathbf{r}_h \\ \mathbf{\Lambda} \end{bmatrix}, \tag{15}$$

where **F** is a $N_h(n+1) \times M_c(n+1)$ measurement matrix, which can be defined as

$$\dot{\mathbf{F}} = \begin{bmatrix}
\hat{y}_{l}(\mathbf{X}^{(1)}) & \psi_{c_{1}}(\mathbf{X}^{(1)}) & \cdots & \psi_{c_{M_{c}}}(\mathbf{X}^{(1)}) & \frac{\partial \psi_{c_{1}}(\mathbf{X}^{(1)})}{\partial x_{1}} & \cdots & \frac{\partial \psi_{c_{1}}(\mathbf{X}^{(1)})}{\partial x_{n}} & \cdots & \frac{\psi_{c_{M_{c}}}(\mathbf{X}^{(1)})}{\partial x_{n}} \\
\hat{y}_{l}(\mathbf{X}^{(2)}) & \psi_{c_{1}}(\mathbf{X}^{(2)}) & \cdots & \psi_{c_{M_{c}}}(\mathbf{X}^{(2)}) & \frac{\partial \psi_{c_{1}}(\mathbf{X}^{(2)})}{\partial x_{1}} & \cdots & \frac{\partial \psi_{c_{1}}(\mathbf{X}^{(2)})}{\partial x_{n}} & \cdots & \frac{\psi_{c_{M_{c}}}(\mathbf{X}^{(2)})}{\partial x_{n}} \\
\vdots & \vdots & \ddots & \vdots & \vdots & \ddots & \vdots \\
\hat{y}_{l}(\mathbf{X}^{(N_{h})}) & \psi_{c_{1}}(\mathbf{X}^{(N_{h})}) & \cdots & \psi_{c_{M_{c}}}(\mathbf{X}^{(N_{h})}) & \frac{\partial \psi_{c_{1}}(\mathbf{X}^{(N_{h})})}{\partial x_{1}} & \vdots & \frac{\partial \psi_{c_{1}}(\mathbf{X}^{(N_{h})})}{\partial x_{n}} & \cdots & \frac{\psi_{c_{M_{c}}}(\mathbf{X}^{(N_{h})})}{\partial x_{n}}
\end{bmatrix}, (16)$$

and \mathbf{R}_h denotes the correlation matrix of high-fidelity samples, \mathbf{r}_h represents the correlation vector between the untried point \mathbf{X} and the observed high-fidelity points \mathbf{S}_h , as given by

$$\dot{\mathbf{R}}_{h} = \begin{bmatrix} R_{h}(\mathbf{X}^{(1)}, \mathbf{X}^{(1)}) & \cdots & R_{h}(\mathbf{X}^{(1)}, \mathbf{X}^{(N_{h}}) & \frac{\partial R_{h}(\mathbf{X}^{(1)}, \mathbf{X}^{(1)})}{\partial x_{1}} & \cdots & \frac{\partial R_{h}(\mathbf{X}^{(1)}, \mathbf{X}^{(N_{h}})}{\partial x_{n}} & \frac{\partial R_{h}(\mathbf{X}^{(1)}, \mathbf{X}^{(N_{h}})}{\partial x_{n}} \\ \vdots & \ddots & \vdots & \ddots & \vdots & \ddots & \vdots \\ R_{h}(\mathbf{X}^{(N_{h})}, \mathbf{X}^{(1)}) & \cdots & R_{h}(\mathbf{X}^{(N_{h})}, \mathbf{X}^{(N_{h})}) & \frac{\partial R_{h}(\mathbf{X}^{(N_{h})}, \mathbf{X}^{(1)})}{\partial x_{1}} & \cdots & \frac{\partial R_{h}(\mathbf{X}^{(N_{h})}, \mathbf{X}^{(1)})}{\partial x_{n}} & \cdots & \frac{\partial R_{h}(\mathbf{X}^{(N_{h})}, \mathbf{X}^{(N_{h})})}{\partial x_{n}} \\ \vdots & \ddots & \vdots & \ddots & \vdots & \ddots & \vdots \\ \frac{\partial R_{h}(\mathbf{X}^{(1)}, \mathbf{X}^{(1)})}{\partial x_{n}} & \cdots & \frac{\partial R_{h}(\mathbf{X}^{(1)}, \mathbf{X}^{(N_{h})})}{\partial x_{n}} & \frac{\partial R_{h}(\mathbf{X}^{(1)}, \mathbf{X}^{(1)})}{\partial x_{n}} & \cdots & \frac{\partial R_{h}(\mathbf{X}^{(1)}, \mathbf{X}^{(N_{h})})}{\partial x_{n}\partial x_{n}} \\ \vdots & \vdots & \vdots & \ddots & \vdots & \ddots & \vdots \\ \frac{\partial R_{h}(\mathbf{X}^{(N_{h})}, \mathbf{X}^{(1)})}{\partial x_{n}} & \cdots & \frac{\partial R_{h}(\mathbf{X}^{(N_{h})}, \mathbf{X}^{(N_{h})})}{\partial x_{n}\partial x_{n}} & \frac{\partial R_{h}(\mathbf{X}^{(1)}, \mathbf{X}^{(1)})}{\partial x_{n}\partial x_{n}} & \cdots & \frac{\partial R_{h}(\mathbf{X}^{(N_{h})}, \mathbf{X}^{(N_{h})})}{\partial x_{n}\partial x_{n}} \\ \vdots & \vdots & \vdots & \ddots & \vdots & \ddots & \vdots \\ \frac{\partial R_{h}(\mathbf{X}^{(N_{h})}, \mathbf{X}^{(1)})}{\partial x_{n}} & \cdots & \frac{\partial R_{h}(\mathbf{X}^{(N_{h})}, \mathbf{X}^{(1)})}{\partial x_{n}\partial x_{n}} & \cdots & \frac{\partial R_{h}(\mathbf{X}^{(N_{h})}, \mathbf{X}^{(N_{h})})}{\partial x_{n}\partial x_{n}} \\ \vdots & \vdots & \vdots & \ddots & \vdots & \ddots & \vdots \\ \frac{\partial R_{h}(\mathbf{X}^{(N_{h})}, \mathbf{X}^{(1)})}{\partial x_{n}} & \cdots & \frac{\partial R_{h}(\mathbf{X}^{(N_{h})}, \mathbf{X}^{(1)})}{\partial x_{n}\partial x_{n}} & \cdots & \frac{\partial R_{h}(\mathbf{X}^{(N_{h})}, \mathbf{X}^{(N_{h})})}{\partial x_{n}\partial x_{n}} \\ \vdots & \vdots & \vdots & \ddots & \vdots & \ddots & \vdots \\ \frac{\partial R_{h}(\mathbf{X}^{(N_{h})}, \mathbf{X}^{(1)})}{\partial x_{n}} & \cdots & \frac{\partial R_{h}(\mathbf{X}^{(N_{h})}, \mathbf{X}^{(N_{h})})}{\partial x_{n}\partial x_{n}} & \cdots & \frac{\partial R_{h}(\mathbf{X}^{(N_{h})}, \mathbf{X}^{(N_{h})})}{\partial x_{n}\partial x_{n}} \\ \vdots & \vdots & \ddots & \vdots & \ddots & \vdots \\ \frac{\partial R_{h}(\mathbf{X}^{(N_{h})}, \mathbf{X}^{(1)})}{\partial x_{n}} & \cdots & \frac{\partial R_{h}(\mathbf{X}^{(N_{h})}, \mathbf{X}^{(N_{h})})}{\partial x_{n}\partial x_{n}} & \cdots & \frac{\partial R_{h}(\mathbf{X}^{(N_{h})}, \mathbf{X}^{(N_{h})})}{\partial x_{n}\partial x_{n}} \\ \vdots & \vdots & \ddots & \vdots & \ddots & \vdots \\ \vdots & \ddots & \vdots & \ddots & \vdots \\ \frac{\partial R_{h}(\mathbf{X}^{(N_{h})}, \mathbf{X}^{(1)})}{\partial x_{n}} & \cdots & \frac{\partial R_{h}(\mathbf{X}^{(N_{h})}, \mathbf{X}^{(N_{h})})}{\partial x_{n}\partial x_{n}} & \cdots & \frac{\partial R_{h}(\mathbf{X}^{(N_{h})}, \mathbf{X}^{(N_{h})})}{\partial x_{n}\partial x_{n}} \\$$

$$\dot{\mathbf{r}}_{h}(\mathbf{X}) = \left\{ \mathbf{r}_{h}(\mathbf{X}) \quad \frac{\partial \mathbf{r}_{h}(\mathbf{X})}{\partial x_{1}} \quad \cdots \quad \frac{\partial \mathbf{r}_{h}(\mathbf{X})}{\partial x_{n}} \right\}^{\mathrm{T}} \in \mathbb{R}^{N_{h}(n+1) \times 1}$$

$$\mathbf{r}_{h}(\mathbf{X}) = \left[R_{h}(\mathbf{X}^{(1)}, \mathbf{X}), R_{h}(\mathbf{X}^{(2)}, \mathbf{X}), \cdots, R_{h}(\mathbf{X}^{(N_{l})}, \mathbf{X}) \right]^{\mathrm{T}}$$
(18)

and

$$\tilde{\boldsymbol{\lambda}} = -\frac{\boldsymbol{\lambda}}{2\sigma_h^2}, \, \boldsymbol{\lambda} = \begin{pmatrix} \lambda_1 & \lambda_2 & \cdots & \lambda_{M_c(n+1)+1} \end{pmatrix}^{\mathrm{T}},$$

$$\dot{\boldsymbol{\Lambda}} = \begin{bmatrix} \hat{y}_l(\mathbf{X}) & \psi_{c_1}(\mathbf{X}) & \psi_{c_2}(\mathbf{X}) & \cdots & \psi_{c_{M_c}}(\mathbf{X}) & \cdots & \frac{\partial \psi_{c_1}(\mathbf{X})}{\partial x_1} & \frac{\partial \psi_{c_{M_c}}(\mathbf{X})}{\partial x_1} & \cdots & \frac{\partial \psi_{c_{M_c}}(\mathbf{X})}{\partial x_n} \end{bmatrix}^{\mathrm{T}},$$

$$(19)$$

where λ is the Lagrange multiplier vector, and $\dot{\Lambda}$ is the trend vector. The reader is referred to [24, 27] about the standard universal Kriging regression process for further details.

Once the weight coefficients \mathbf{w} are obtained by solving Eq. (15), the GEMF-PCK predictor at any untried point \mathbf{X} is given by

$$\hat{\mathbf{y}}_{h}(\mathbf{X}) = \alpha_{0}\hat{\mathbf{y}}_{l}(\mathbf{X}) + \sum_{i=1}^{M_{c}} \alpha_{c_{i}} \psi_{c_{i}}(\mathbf{X}) + \sum_{i=1}^{M_{c}} \sum_{j=1}^{n} \alpha_{c_{i,j}} \frac{\partial \psi_{c_{i}}(\mathbf{X})}{\partial x_{i}} + \dot{\mathbf{r}}_{h}^{\mathrm{T}}(\mathbf{X})\dot{\mathbf{R}}_{h}^{-1} (\dot{\mathbf{Y}}_{h} - \dot{\mathbf{F}}\dot{\boldsymbol{\alpha}}), \tag{20}$$

where $\hat{y}_l(\mathbf{X})$ is the predictor of LF PCK model, and M_c ($M_c \leq M$) denotes the number of polynomial terms in the correction expansion. The coefficients vector $\dot{\boldsymbol{\alpha}} = (\alpha_0, \alpha_{c_1}, \alpha_{c_2}, \alpha_{c_{M_c}}, \alpha_{c_{1,1}}, \cdots, \alpha_{c_{1,n}}, \cdots, \alpha_{c_{M_c,n}})^T$ can be estimated by GLSE method namely

$$\dot{\boldsymbol{\alpha}} = \left(\dot{\mathbf{F}}^{\mathrm{T}}\dot{\mathbf{R}}_{h}^{-1}\dot{\mathbf{F}}\right)^{-1}\dot{\mathbf{F}}^{\mathrm{T}}\dot{\mathbf{R}}_{h}^{-1}\dot{\mathbf{Y}}_{h},\tag{21}$$

where the first column and other columns of \mathbf{F} (Eq. (16)) are calculated by substituting the observed point set \mathbf{S}_h into $\hat{y}_l(\mathbf{X})$ and $\psi_{c_l}(\mathbf{X})$ ($i=1,2,\cdots,M_c$), respectively. The unknown hyper-parameters $\mathbf{\theta}_h$ and q_h of the correlation function $\dot{\mathbf{R}}_h$ are tuned by minimizing the condensed likelihood expression (MLE)

$$\left\{\boldsymbol{\theta}_{h}, q_{h}\right\}_{ML} = \underset{\boldsymbol{\theta}_{h}, q_{h}}{\min} \left(\sigma_{z_{h}}^{2} \left|\dot{\mathbf{R}}_{h}\right|^{1/N_{h}}\right), \ \theta_{h_{h}} > 0, q_{h} > 0,$$

$$(22)$$

where the stationary process variance $\sigma_{z_h}^2$ can be estimated by $\hat{\sigma}_{z_h}^2 = (\dot{\mathbf{Y}}_h - \dot{\mathbf{F}}\dot{\alpha})^{\mathrm{T}}\dot{\mathbf{R}}_h^{-1}(\dot{\mathbf{Y}}_h - \dot{\mathbf{F}}\dot{\alpha})/N_h$. Then, the correlation matrix $\dot{\mathbf{R}}_h$ and correlation vector $\dot{\mathbf{r}}_h$ are calculated by substituting the corresponding high-fidelity samples sites \mathbf{S}_h and optimized hyper-parameters $\mathbf{\theta}_h$ and q_h , as defined in Eq. (19). Further, we can get the MSE of the GEMF-PCK predictor at the untried point \mathbf{X} as

$$s_{y_h}^2(\mathbf{X}) = \sigma_{z_h}^2 \left(1.0 - \dot{\mathbf{r}}_h^{\mathrm{T}} \dot{\mathbf{R}}_h^{-1} \dot{\mathbf{r}}_h + \dot{\boldsymbol{\Gamma}} \left(\dot{\mathbf{F}}^{\mathrm{T}} \dot{\mathbf{R}}_h^{-1} \dot{\mathbf{F}} \right)^{-1} \dot{\boldsymbol{\Gamma}}^{\mathrm{T}} \right), \tag{23}$$

where $\dot{\mathbf{\Gamma}} = \dot{\mathbf{r}}_h^\mathrm{T} \dot{\mathbf{R}}_h^{-1} \dot{\mathbf{F}} - \dot{\mathbf{\Lambda}}^\mathrm{T}$. The GEMF-PCK approach calculates the correlation matrix \mathbf{R}_h and \mathbf{R}_l with less complexity and smaller sizes compared to traditional co-Kriging method [10, 24, 28].

3. Multidisciplinary robust design frame

To effectively solve the robust aerodynamic/stealth design optimization problem, an efficient optimization framework is elaborated, as shown in Fig. 1. In this framework, once the GEMF-PCK metamodel $\hat{y}_h(\mathbf{X}_{\Xi})$ is built, as presented in the next section, the designers can apply $\hat{y}_h(\mathbf{X}_{\Xi})$ to estimate the statistical characteristics of each candidate design in UBDO routine. Let $\{\Xi^{(i)}\}_{i=1}^{N_m}$ denote the sample of RVs generated by a DOE according to PDFs of RVs. The first two moments of HF function response at each design \mathbf{X} considering the effect of uncertainty are given by

$$\mu_{y}(\mathbf{X}) = \frac{1}{N_{m}} \sum_{i=1}^{N_{m}} \hat{y}_{h}(\mathbf{X}, \mathbf{\Xi}^{(i)}), \sigma_{y}(\mathbf{X}) = \sqrt{\frac{1}{N_{m} - 1} \sum_{i=1}^{N_{m}} (\hat{y}_{h}(\mathbf{X}, \mathbf{\Xi}^{(i)}) - \mu_{y}(\mathbf{X}))^{2}},$$
(24)

where N_m is the number of sampling the MF PC-Kriging predictor $\hat{y}_h(\mathbf{X}, \mathbf{\Xi})$ and it should be sufficient to meet the desirable accuracy of moment propagation and probability analysis. In addition, the probability of violating the constraint function \mathbf{g}_h can also be estimated by

$$P_{g} = \frac{1}{N_{m}} \sum_{i=1}^{N_{m}} I^{(i)}, \quad I^{(i)} = I(\mathbf{X}, \mathbf{\Xi}^{(i)}) = \begin{cases} 1 & \text{if } \hat{g}_{h}(\mathbf{X}, \mathbf{\Xi}^{(i)}) < 0 \\ 0 & \text{if } \hat{g}_{h}(\mathbf{X}, \mathbf{\Xi}^{(i)}) \ge 0 \end{cases}, \quad i = 1, 2, \dots, N_{m},$$
 (25)

wherein $\hat{g}_h(\mathbf{X}, \mathbf{\Xi})$ denotes the MF PC-Kriging predictor of HF function $g_h(\mathbf{X}, \mathbf{\Xi})$ with $g_h \geq 0$ required for feasible designs. For general applications, the moment matching formulation [29] can rapidly estimate the feasible robustness by using the estimated mean μ_g and standard deviation σ_g of the constraint. Such formulation is also widely used, e.g., the popular six sigma method haves less than 3.4 failures per million possibilities and three-sigma method with a success rate of 93%.

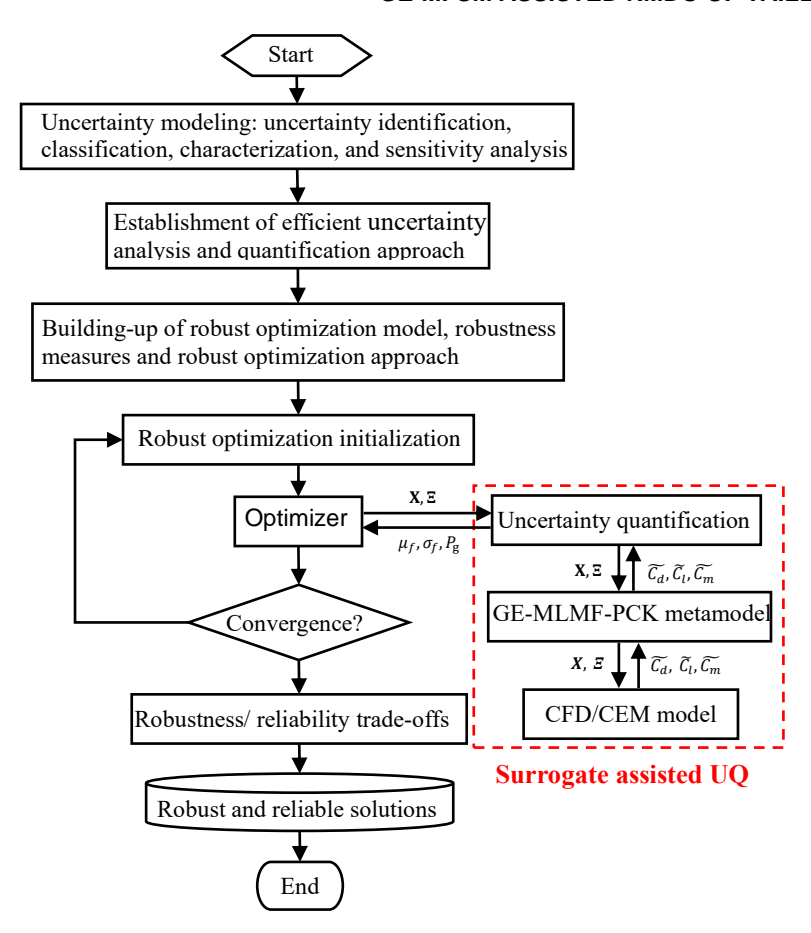


Fig. 1 the flowchart of robust aerodynamic/stealth design optimization framework

4. Robust aerodynamic/stealth design of tailless flying wing shape

The aerodynamic design optimization of a tailless flying wing configuration is a significant challenge to these traditional aerodynamic shape design optimization methods. This is because thus shape requires maintaining a balance of longitudinal moments of this configuration while it simultaneously seeks to satisfy the requirements for full-frequency omnidirectional stealth and good aerodynamic characteristics under a wide range of Mach numbers as well as high load capacity. Through computational analyses of this type of tailless flying wing configuration, it is found that these complex design requirements and constraints can usually be accomplished by the collaborative design of the inner and outer wing segments. The inner flying wing segment of the flying wing mainly fulfills the design requirements for balancing the node down pitching moment, maintaining high stealth and good load characteristics. The outer flying wing segment mainly meets the drag-reduction requirements for transonic cruise to improve the cruise efficiency. Therefore, good subsonic aerodynamic/stealth characteristics require the cooperation of the inner and outer wing segments. which impose different design requirements and constraints on the airfoils of the inner and outer wing segments, respectively. Therefore, the design of the flying wing airfoils for the double swept flying wing shape is a typical multidisciplinary and multi-objective design problem that integrates aerodynamic, stealth, and flight control characteristics. In this paper, this initial model, that is similar to X-47B in size and configuration, is assembled the NACA 65,3-014 series airfoils in the inner, middle, and outer wing sections, respectively. The initial model and three-dimensional FFD parameterization frame are shown in Fig. 2. The multidisciplinary robust design optimization model considering Mach number and lift coefficient uncertainty is given as

Condition: Re =
$$6.8 \times 10^{6}$$
, $Ma_{\infty} \in U[0.76, 0.83]$, $C_{L} \in U[0.1, 0.3]$
Find: $\mathbf{X} \in \mathbb{R}^{n}$, $\mathbf{X} \in [\mathbf{X}_{L}, \mathbf{X}_{U}]$
Minimize:
$$\begin{cases} \lambda_{1}u_{c_{d}}(Ma_{\infty}, C_{L}) + \lambda_{2}u_{RCS} + \lambda_{3} |u_{c_{m}}| \\ \lambda_{4}\sigma_{C_{d}}(Ma_{\infty}, C_{L}) + \lambda_{5}\sigma_{RCS} + \lambda_{6}\sigma_{c_{m}} \end{cases}$$

$$Subject to: t_{\max} / c_{root} \geq t_{\max} / c_{root, initial}$$

$$t_{\max} / c_{kink} \geq t_{\max} / c_{kink, initial}$$

$$t_{\max} / c_{tip} \geq t_{\max} / c_{tip, initial}$$
(26)

wherein, the first object of this model is the weighted mean sum of drag coefficient (\mathcal{C}_d), pitching moment coefficient (\mathcal{C}_m), the average horizontal RCS (HH) in the frontal sector. The second objective is the weighted stand deviation sum of drag coefficient, pitching moment coefficient, the average horizontal RCS (HH) in the frontal sector, subject to the thickness of these three wing sections.

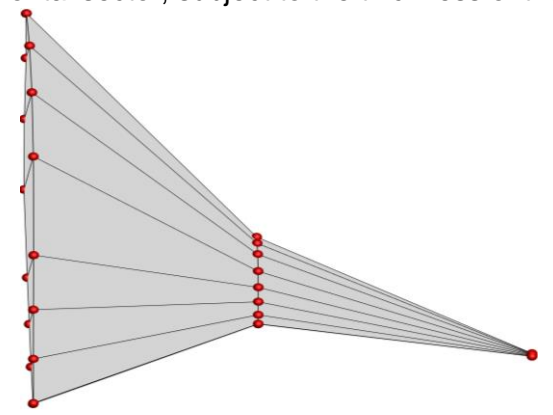


Fig. 2 Surface grid and free form deformation frame for the initial model

This example uses the SST turbulence model for aerodynamic evaluation, which gets an initial drag coefficient of 133.55 counts. The classical MOEA/D algorithm is used for multi-objective optimization. A compromise based on the self-organizing map is made to obtain the best shape of robust design. The comparison between the initial wing sections and the optimized wing sections is shown in Fig. 3. Fig. 4-Fig. 7 compare the drag divergence curves and moment coefficient curves at lift coefficients from 0.1 to 0.25. The results show that the robust design wing achieves lower drag coefficients over a range of Mach number and a higher drag-divergence Mach number compared to the initial shape. Meantime, the pitching moment coefficients (C_m) of the robust design wing are approach to zero while the initial wing with larger values of \mathcal{C}_m , that means the robust design wing achieves a significant improvement in aerodynamic characteristics while maintaining good longitudinal moment self-balancing capabilities. When the Mach number is greater than 0.8, compared to the initial wing, the robust design wing achieves average drag coefficients reduction of more than 20 counts and an increased drag-divergence Mach number of more than 0.03. Fig. 8 compare the probability density function (PDF) curves of drag coefficients and pitching moment coefficients between the initial wing and the robust design wing, which indicates that the robust design wing achieves considerably lower mean and standard deviation of drag coefficient, as well as smaller mean of pitching moment coefficient, close to 0. Therefore, the aerodynamic characteristics of the robust design wing are significantly improved compared to the initial wing. The robustness of the drag coefficient and pitching moment coefficient of the robust design wing is significantly improved compared to the initial wing. Further, the robust design wing achieves a larger range of low drag coefficients and a higher feasible robustness of the pitching moment coefficient.

Fig. 9-Fig. 10 compare the pressure distributions clouds on the upper surface between the initial wing and robust design wing at four different flight conditions. Results indicate that the robust design wing has flatter pressure distribution and weaker shock waves on the upper surface of the inner wing

GE-MFSM ASSISTED RMDO OF TAILLESS FLYING WING

section, resulting in significant reductions in wave drag and pressure drag. Figure 11 shows the comparison of the RCS curves between the initial wing and the robust design wing at L, S, C, and X bands. They demonstrate that the robust design wing significantly reduces the horizontal RCS (HH)and vertical RCS (VV) compared to the initial wing, with the concerned RCS of the front threat sector, that is $\phi = -90^{\circ} - 90^{\circ}$, reduced by more than one order of magnitude, and the average RCS reduced by more than 90%. The results reveal that the robust design wing achieves a significant improvement in all-frequency omnidirectional RCS and is capable of meeting the future requirements for designing a high-stealth flying wing shape. The robust design optimization results verify the reliability and effectiveness of the proposed multidisciplinary robust design optimization method compared to traditional deterministic design methods, laying the foundation for the development of advanced aerodynamic configuration design method for engineering usage.

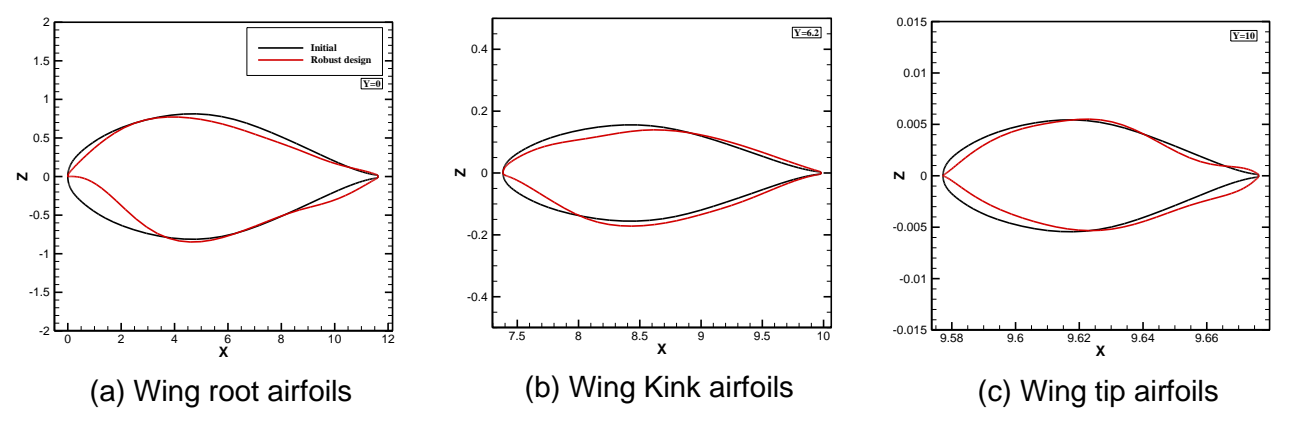


Fig. 3 Airfoils comparisons at different sections of initial shape and robust design shape.

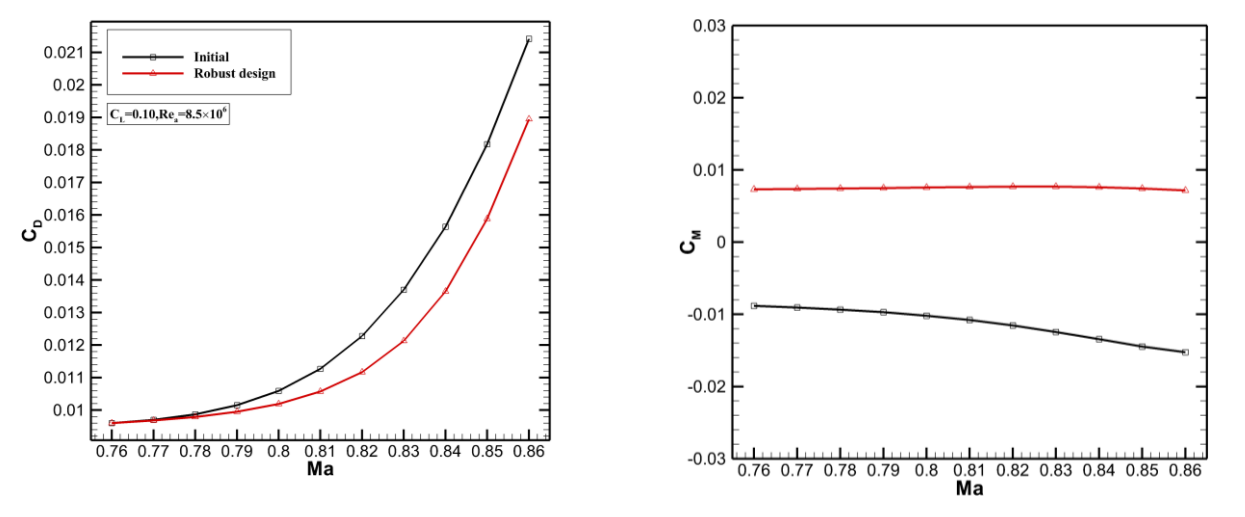
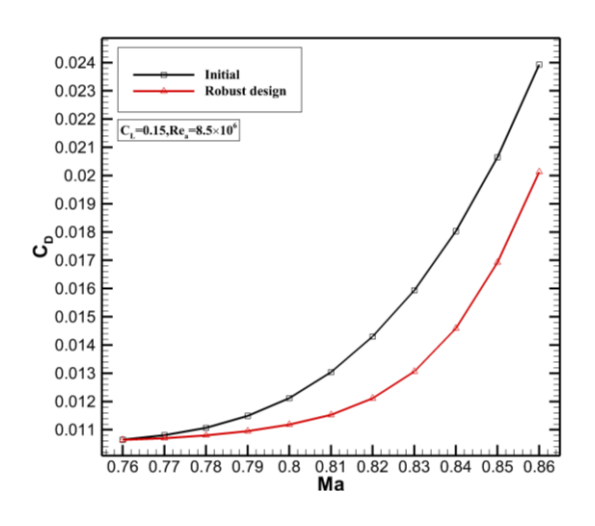


Fig. 4 Comparisons of drag-divergence Mach number and pitching moment coefficients between initial shape and robust design shape at $C_L = 0.10$



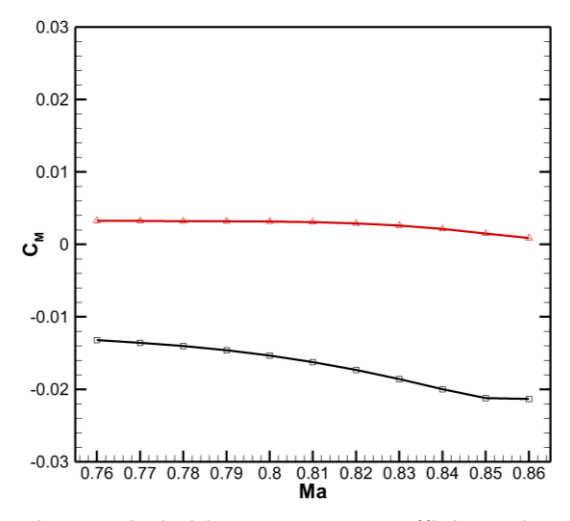
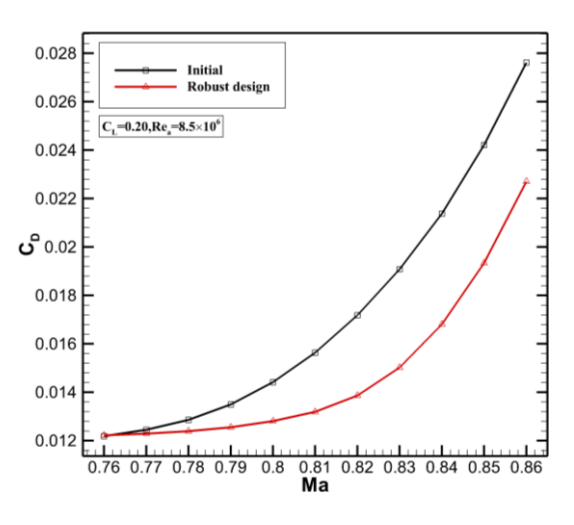


Fig. 5 Comparisons of drag-divergence Mach number and pitching moment coefficients between initial shape and robust design shape at $C_L = 0.15$.



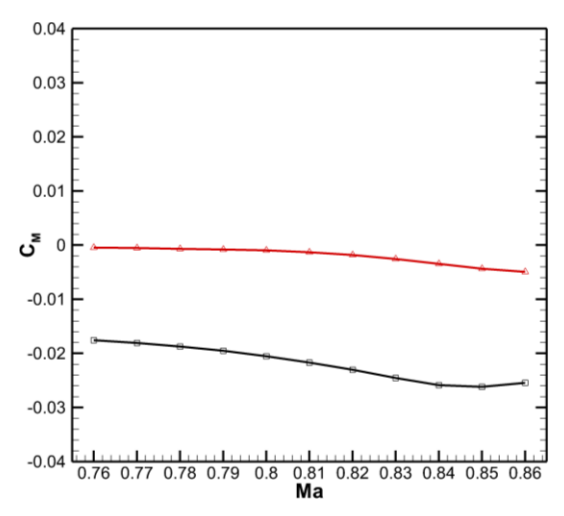
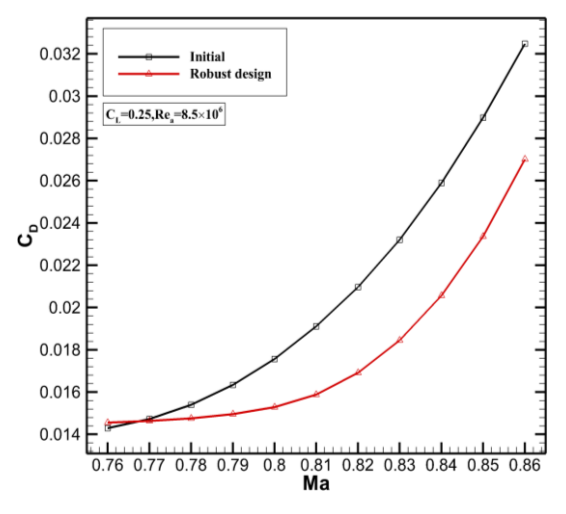


Fig. 6 Comparisons of drag-divergence Mach number and pitching moment coefficients between initial shape and robust design shape at $C_L=0.20$



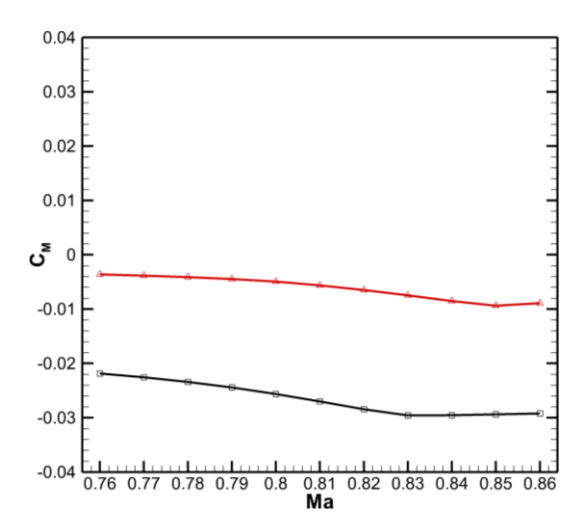
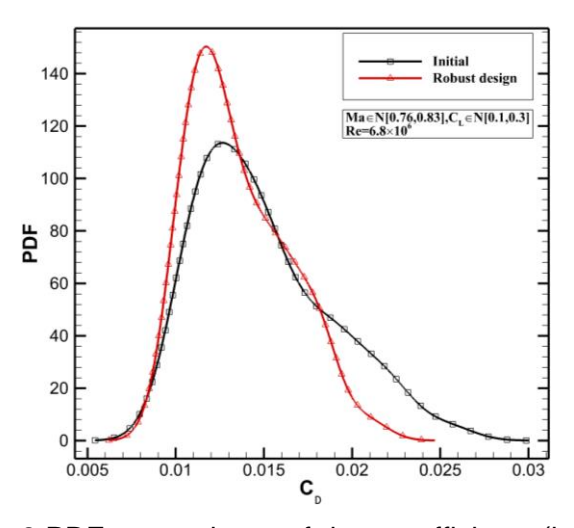


Fig. 7 Comparisons of drag-divergence Mach number and pitching moment coefficients between initial shape and robust design shape at $C_L = 0.25$



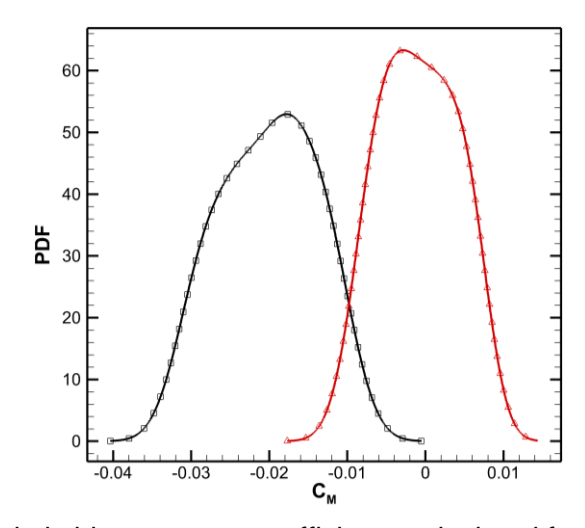
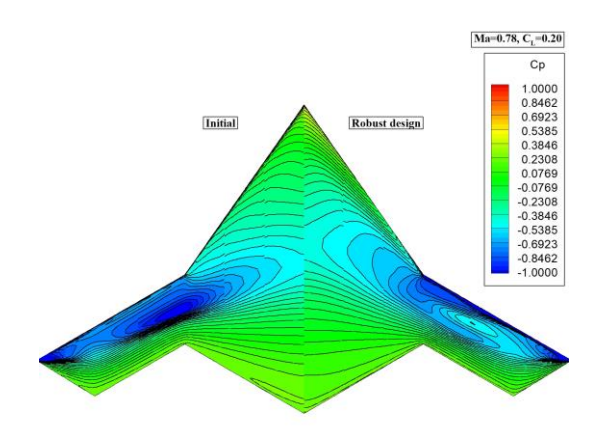


Fig. 8 PDF comparisons of drag coefficients (left) and pitching moment coefficients calculated from initial shape and robust design shape.



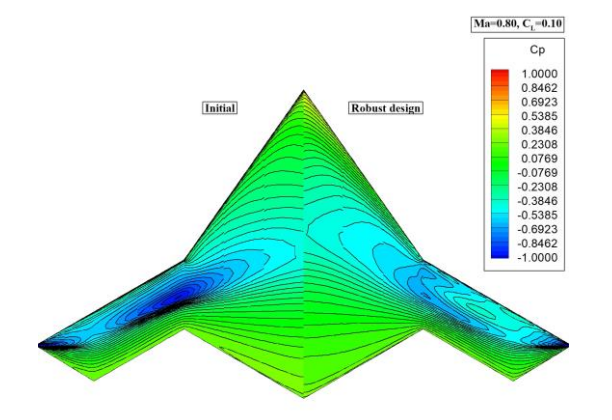
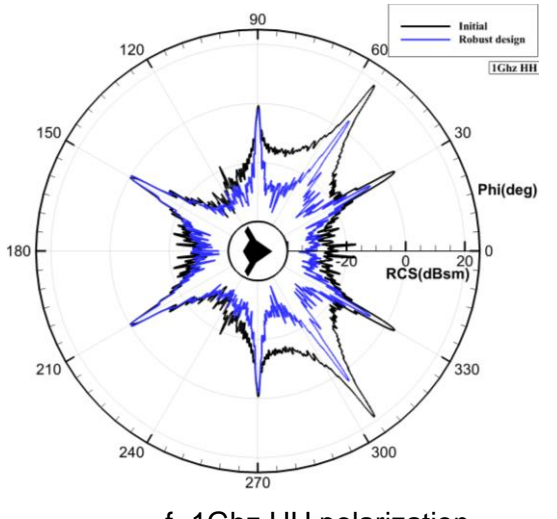
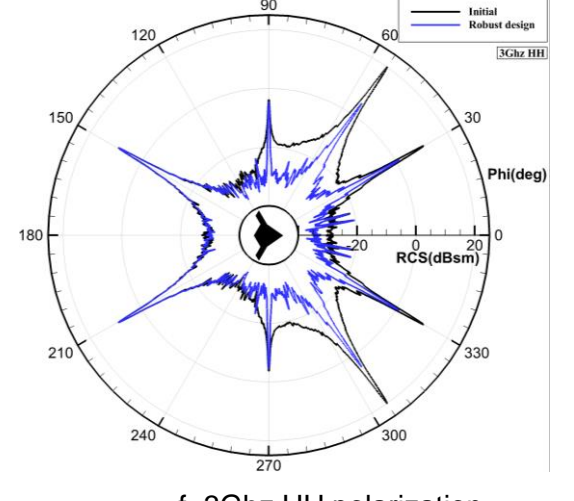


Fig. 9 Comparison of pressure coefficients distributions between initial shape and robust design shape ($Ma_{\infty}=0.78, C_L=0.20$)

Fig. 10 Comparison of pressure coefficients distributions between initial shape and robust design shape ($Ma_{\infty}=0.80, C_L=0.10$)





f=1Ghz HH polarization

f=3Ghz HH polarization

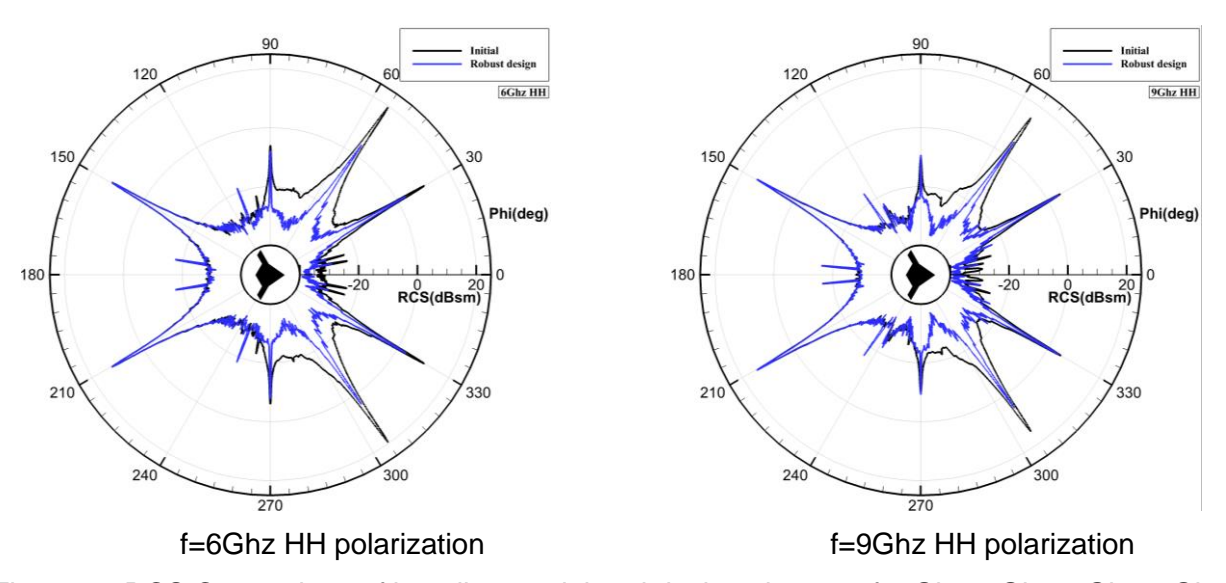


Figure 11 RCS Comparison of baseline model and design shape at f=1Ghz, 3Ghz, 6Ghz, 9Ghz HH polarization, respectively.

5. Conclusion

This article proposes an efficient single cycle robust aerodynamic/stealth design optimization method based on a novel gradient-enhanced multi-fidelity polynomial chaos-Kriging (GEMF-PCK) surrogate model to address the challenge of huge computational costs from current robust design methods. The new GEMF-PCK model has been fully validated, with significantly higher modeling efficiency and accuracy compared to popular surrogate models such as universal Kriging, PC-Kriging, and Co-Kriging. In particular, it significantly improves the generalization ability and global learning ability for highly-nonlinear/high-order aerodynamic responses, resulting in a more stable and reliable modelling process. To validate the performance of the developed method, a complex aerodynamic/stealth multidisciplinary robust design of the tailless flying wing shape is conducted. Results show that the developed aerodynamic/stealth multi-objective robust design optimization method significantly improves the optimization efficiency, meeting the needs of efficient aerodynamic/stealth design for the future tailless flying wing. The optimized new shape reduces the average drag by more than 20 counts over a wide Mach number range compared to the initial layout, increases the Mach number of drag divergence by 0.03, and significantly improves the robustness of drag coefficient. The longitudinal moment coefficient of the whole aircraft reaches self-leveling, and the reliability is also significantly higher. At the same time, stealth analysis shows that compared to the initial layout, the optimized layout reduces the average radar cross section (RCS) by more than 90% in the L, S, C, X bands, and reduces the forward RCS by more than one order of magnitude, resulting in comprehensive improvement in stealth characteristics, which can meet the needs of future highstealthy flying wing layout aircraft for all-directional and all-frequency stealthy use.

6. Contact Author Email Address

Zhao Huan, huanzhao@nwpu.edu.cn

7. Copyright Statement

The authors confirm that they, and/or their company or organization, hold copyright on all of the original material included in this paper. The authors also confirm that they have obtained permission, from the copyright holder of any third-party material included in this paper, to publish it as part of their paper. The authors confirm that they give permission, or have obtained permission from the copyright holder of this paper, for the publication and distribution of this paper as part of the ICAS proceedings or as individual off-prints from the proceedings.

References

- [1] Bons N P, He X, Mader C A, Martins J R. Multimodality in aerodynamic wing design optimization [J]. *AIAA Journal*, 2019, 57(3): 1004-1018.
- [2] Poole D, Allen C, Rendall T. Global optimization of wing aerodynamic optimization case exhibiting multimodality [J]. *Journal of Aircraft*, 2018, 55(4): 1576-1591.
- [3] Chernukhin O, Zingg D W. Multimodality and global optimization in aerodynamic design [J]. *AIAA journal*, 2013, 51(6): 1342-1354.
- [4] Zhao Huan, Huang Yu Jun, Xing Hao Nan. Adaptive sparse polynomial chaos-based flow field/sonic boom uncertainty quantification under multi-parameter uncertainties[J]. *Chinese Journal of Theoretical and Applied Mechanics*, 2023, 55(9): 2027-2042(in Chinese). DOI: 10.6052/0459-1879-23-122.
- [5] Forrester A I, Sóbester A, Keane A J. Multi-fidelity optimization via surrogate modelling [J]. *Proceedings of the royal society a: mathematical, physical and engineering sciences*, 2007, 463(2088): 3251-3269.
- [6] Peherstorfer B, Willcox K, Gunzburger M. Survey of multifidelity methods in uncertainty propagation, inference, and optimization [J]. *SIAM Review*, 2018, 60(3): 550-591.
- [7] Fernández-Godino M G, Park C, Kim N H, Haftka R T. Issues in Deciding Whether to Use Multifidelity Surrogates [J]. *AIAA Journal*, 2019, 57(5): 2039-2054.
- [8] Toal D J. Some considerations regarding the use of multi-fidelity Kriging in the construction of surrogate models [J]. *Structural and Multidisciplinary Optimization*, 2015, 51(6): 1223-1245.
- [9] Zhao H, Gao Z, Xu F, Xia L. Adaptive multi-fidelity mparse polynomial chaos-Kriging metamodeling for global approximation of aerodynamic data [J]. *Structural and Multidisciplinary Optimization*, 2021, 1-40.
- [10] Kennedy M C, O'Hagan A. Predicting the output from a complex computer code when fast approximations are available [J]. *Biometrika*, 2000, 87(1): 1-13.
- [11]Palar P S, Tsuchiya T, Parks G T. Multi-fidelity non-intrusive polynomial chaos based on regression [J]. *Computer Methods in Applied Mechanics & Engineering*, 2016, 305(579-606.
- [12] Ng L W-T, Eldred M. Multifidelity uncertainty quantification using non-intrusive polynomial chaos and stochastic collocation [C]. Proceedings of the 53rd AIAA/ASME/ASCE/AHS/ASC Structures, Structural Dynamics and Materials Conference 20th AIAA/ASME/AHS Adaptive Structures Conference 14th AIAA, 2012: 1852.
- [13] Zhao H, Gao Z, Xu F, Xia L. Adaptive multi-fidelity sparse polynomial chaos-Kriging metamodeling for global approximation of aerodynamic data [J]. *Structural and Multidisciplinary Optimization*, 2021, 64(2): 829-858.
- [14] Zhao H, Gao Z-H, Xia L. Efficient aerodynamic analysis and optimization under uncertainty using multi-fidelity polynomial chaos-Kriging surrogate model [J]. *Computers & Fluids*, 2022, 246(105643.
- [15] Zhao Huan. Adaptive multi-fidelity polynomial chaos-kriging model-based efficient aerodynamic design optimization method. *Chinese Journal of Theoretical and Applied Mechanics*, 2023, 55(1): 223.
- [16] Zhao Huan, Gao Zheng Huan, Xia Lu. Research on novel multi-fidelity surrogate model assisted many-objective optimization method [J]. *Acta Aeronautica et Astronautica Sinica*, 2023, 44(2):126962(in Chinese). doi: 10.7527/S1000-6893.2022.26962, 2023, 44(6): 127038.
- [17] Zhao Huan, Gao Zheng Hong, Xia Lu. Research on efficient robust aerodynamic design optimization method of high-speed and high-lift NLF airfoil [J]. *Acta Aeronautica et Astronautica Sinica*, 2021, 42(7): 124894 (in Chinese). doi: 10.7527/S1000-6893.2020.24894., 2022, 43(1): 124894-124894.
- [18] Zhao H, Gao Z, Xu F, Zhang Y. Review of Robust Aerodynamic Design Optimization for Air Vehicles [J]. *Archives of Computational Methods in Engineering*, 2019, 26(3): 685-732.
- [19] Zhao H, Gao Z, Xu F, Zhang Y, Huang J. An efficient adaptive forward–backward selection method for sparse polynomial chaos expansion [J]. *Computer Methods in Applied Mechanics and Engineering*, 2019, 355(456-491.
- [20] Zhao H, Gao Z. Uncertainty-based design optimization of NLF airfoil for high altitude long endurance unmanned air vehicles [J]. *Engineering Computations*, 2019, 36(3): 971-996.
- [21] Zhao H, Gao Z. Robust design optimization of benchmark aerodynamic case based on polynomial chaos expansion [C]. *Proceedings of the 31st Congress of the International Council of the Aeronautical Sciences*, ICAS 2018, 2018.
- [22] Marrel A, Iooss B, Van Dorpe F, Volkova E J C S, Analysis D. An efficient methodology for modeling complex computer codes with Gaussian processes [J]. *Computational Statistics & Data Analysis*, 2008,

- 52(10): 4731-4744.
- [23] Bachoc F J C S, Analysis D. Cross validation and maximum likelihood estimations of hyper-parameters of Gaussian processes with model misspecification [J]. *Computational Statistics & Data Analysis*, 2013, 66(55-69).
- [24] Santner T J, Williams B J, Notz W, Williams B J. The design and analysis of computer experiments [M]. *Springer*, 2003.
- [25] Fernández-Godino M G, Park C, Kim N H, T.Haftka: R. Review of multi-fidelity models [J]. arXiv (160907196v3), 2017.
- [26] Rockafellar R T. Lagrange Multipliers and Optimality [J]. SIAM Review, 2005.
- [27] Zimmerman D, Pavlik C, Ruggles A, Armstrong M P. An experimental comparison of ordinary and universal kriging and inverse distance weighting [J]. *Mathematical Geology*, 1999, 31(4): 375-390.
- [28] Bertram A, Zimmermann R. Theoretical investigations of the new Cokriging method for variable-fidelity surrogate modeling [J]. *Advances in Computational Mathematics*, 2018, 44(6): 1693-1716.
- [29] Parkinson A, Sorensen C, Pourhassan N. A General Approach for Robust Optimal Design [J]. *Journal of Mechanical Design*, 1993, 115(1): 74-80.